Available online at www.sciencedirect.com
SCIENCE DIRECT
Journal of Catalysis 232 (2005) 127–136
JOURNAL OF CATALYSIS
www.elsevier.com/locate/jcat

The effect of Mo oxides and TiO_2 support on the chemisorption features of linearly adsorbed CO on Pt crystallites: an infrared and photoelectron spectroscopy study

S. Zafeiratos, G. Papakonstantinou, M.M. Jacksic, S.G. Neophytides *

Foundation of Research and Technology Hellas, Institute of Chemical Engineering and High Temperature Processes, FORTH-ICE/HT, PO Box 1414, GR-26504 Rion Achaias, Patras, Greece

Received 19 August 2004; revised 24 February 2005; accepted 1 March 2005

Available online 7 April 2005

Abstract

CO adsorption was studied on Pt and Pt_x–Mo ($x = 1$, 4) catalysts supported on TiO_2 by means of temperature-programmed desorption (TPD) and diffuse reflectance Fourier transform infrared spectroscopy (DRIFTS), and significant information on the structure, arrangement, and chemical state of Pt and Mo on the TiO_2 support was obtained by a combination of XPS, H_2 chemisorption, and DRIFTS. It was concluded that the Mo oxide species forms a solid solution with Pt, while a significant part of the Pt surface atoms are screened by two-dimensional Mo oxide nanoclusters. This structural arrangement results in the modification of the chemisorptive properties of Pt, and XPS measurements show that it is partially oxidized; this oxidation state is closely related to the concentration of hydroxyl species on the catalyst's surface. TPD experiments carried out under He flow had shown that the linearly adsorbed CO_L species on the Pt_x–Mo/TiO_2 samples desorbs at temperatures below 375 K, which is almost 100 K below the CO_L species desorption from Pt/TiO_2. This low desorption temperature of CO was attributed to its chemical oxidation at the boundaries of the Mo oxide nanoclusters by the OH species supplied by $MoO(OH)_3$, which was detected by XPS as the most abundant oxidation state. In addition, the execution of TPD experiments under H_2 flow resulted in the desorption of the CO_L species for all three samples at significantly higher temperatures, 460, 425, and 390 K, for Pt/TiO_2, Pt–Mo/TiO_2, and Pt_4–Mo/TiO_2, respectively.

Keywords: PtMo electroctatalyst; Fuel cells; TiO_2 support; CO chemisorption; DRIFTS

1. Introduction

Titanium dioxide-supported platinum is one of the most investigated systems in the area of model and realistic metal/metal–oxide systems. This interest has been stimulated by the promotional effect of Pt in photocatalysis, its use as an oxygen gas-sensor system, and the fact that it is a classic strong metal support interaction (SMSI) system with many catalytic applications [1]. Of special interest is the dehydrogenation of organic compounds in a fuel processor or reformer as an attractive way to generate hydrogen that powers fuel cells by converting chemical into electrical energy [2]. The electrocatalytic properties of Pt/TiO_2 are also under study to probe its potential use as a reliable electrocatalyst for low-temperature polymer electrolyte membrane (PEM) fuel cell applications [3,4].

It is well known that the use of Pt as an electrocatalyst in low-temperature PEM fuel cells gives rise to a major problem. The Pt metal surface is easily poisoned by trace amounts of CO [2]. Binary (alloys or segregated metal particles) Pt–M catalysts (where M = Ru, Sn, Re, Rh, or Mo) have received considerable attention as promising catalysts to increase the efficiency of CO oxidation on Pt [5]. Furthermore, the most important issues in contemporary fuel-cell electrocatalysis are related to developing a material that either oxidizes CO or adsorbs a limited amount of CO while

* Corresponding author. Fax: +30 2610 965223.
E-mail address: neoph@iceht.forth.gr (S.G. Neophytides).

0021-9517/$ – see front matter
doi:10.1016/j.jcat.2005.03.003

still being capable of oxidizing hydrogen at an acceptable rate.

Of the Pt–M binary systems, Pt–Ru has been studied in the greatest detail, as this is still one of the most stable and active CO-tolerant catalysts under practical conditions. The origin of the role of Ru is not yet completely understood; however, it is now widely accepted that the mechanism by which CO is removed from the PtRu surface is the so-called bifunctional mechanism suggested by Watanabe and Motoo [6,7]. According to this mechanism, CO adsorbed on Pt is oxidized preferentially by an oxygen-containing surface species as adsorbed OH_{ad}. Although the exact nature of this oxidic species is not yet clear, the role of Ru is to provide nucleation sites for the aforementioned oxygen-containing species. An alternative explanation is the so-called ligand effect, where M influences the Pt–CO bonding by affecting the electronic structure of the binding site on Pt [8,9]. Unfortunately, the interest in Ru as an additive in fuel-cell catalysts is reduced somewhat by its high price and limited availability. This is why the substitution of other, cheaper and more abundant additives for Ru has been suggested [10].

Molybdenum seems to be one of these potentially interesting additives, since it is inexpensive and largely available. Furthermore, recent experimental and theoretical studies have suggested that Pt–Mo could be a better catalyst for CO oxidation than Pt–Ru [10–13]. This enhanced performance that contrasts with Pt–Ru was ascribed to the lack of adsorption of CO on Mo, which leaves more adsorption sides for oxygen-containing species that are acting as CO oxidation reagents (in the framework of a bifunctional mechanism), or to changes in the Pt–Pt atomic distance, which modify the Pt–CO adsorption energy [12].

In the present communication, the adsorption of CO on well-characterized Pt, Pt–Mo, and Pt_4–Mo catalysts supported on TiO_2 is discussed. The CO adsorption was followed by temperature-programmed infrared spectroscopy under He and H_2 atmospheres, and the catalyst's chemical state was characterized ex situ in ultra-high-vacuum conditions by X-ray photoelectron spectroscopy. It will be shown that Mo additives significantly modify CO adsorption/desorption characteristics on Pt, leading to lower CO desorption temperatures as compared with monometallic Pt/TiO_2 catalysts.

2. Experimental

2.1. Catalyst preparation

Pt–Mo/TiO_2 catalysts were prepared via wet impregnation of Pt and MoO_2 acetylacetonates (Aldrich Chem. Co) on TiO_2, anatase (Hombikat Sachtleben; surface area = 200 m^2/g). After drying, the catalyst precursors were loaded into the DRIFTS reactor cell and were treated in flowing H_2/Ar mixture; the temperature was varied at a ramp rate of 2°/min up to 570 K. The sample was kept at 570 K for 2 h. After treatment the sample was cooled to room temperature under the same H_2/Ar flow with a cooling rate of 2°/min. Two Pt/TiO_2 samples of 5 and 10 wt% Pt loading were prepared. The Pt/TiO_2 and Pt–Mo/TiO_2 samples were prepared with a constant total metal loading of 5 wt%. Two Pt_xMo samples with Pt/Mo atomic ratios of $x = 1$ and 4 were investigated, and monometallic 5 wt% Pt/TiO_2 and Mo/TiO_2 were also prepared and measured for comparison.

2.2. XPS and hydrogen chemisorption measurements

XP spectra were collected in an UHV chamber (base pressure 8×10^{-10} mbar) equipped with a hemispherical electron energy analyzer and a twin-anode X-ray gun, which has been described elsewhere [14]. The sample, which was mounted on a transfer rod probe, could be easily transferred from the load lock chamber, where it could be treated with gases at atmospheric pressure and elevated temperatures, into the UHV chamber. The nonmonochromatized Al-K_α line at 1486.6 eV and a constant pass energy mode for the analyzer were used in the experiments. Pass energies of 97 eV resulted in a half width at half-maximum (FWHM) of 1.8 eV for the Au $4f_{7/2}$ peak of a reference foil. The energy scale of the spectrometer was calibrated with both the Au $4f_{7/2}$ line at 84.0 eV and the Ni $2p_{3/2}$ line at 852.4 eV of carefully cleaned polycrystalline Au and Ni foils, respectively. The sample temperature was measured with a Ni–CrNi thermocouple, which was mounted in the sample holder. Curve fitting was performed with a least-squares curve-fitting program based on a mixed Gaussian/Lorentzian function, which accounted for the band asymmetry to higher binding energies in the core level spectra of metallic species. All spectra were obtained at room temperature, after the sample was heated at 570 K under a H_2 atmosphere for 30 min, and the binding energies (BE) were referenced to the C 1s line at 284.6 eV, which was always present because of unavoidable carbon contamination. The uncertainty in the determination of the binding energy values was estimated to be 0.1 eV, and that in calculated atomic ratios was about 10%.

Adsorption experiments were performed in a conventional glass volumetric system (Quantachrome Autosorb-1) in a hydrogen pressure range from 0–80 to 800 mmHg, after being reduced in situ in flowing hydrogen and outgassed at 520 K.

2.3. DRIFTS and temperature-programmed DRIFTS studies

Diffuse reflectance infrared Fourier transform spectroscopy (DRIFTS) measurements were performed in a Bruker (Equinox 55) FTIR spectrometer. The powdered catalysts were placed on the sample holder of a small internal volume (~ 2 cm^3) homemade diffuse reflectance IR cell reactor sealed with a ZnSe window. The gases at the outlet of the IR cell reactor were analyzed with a QMS (Omnistar). The cell

allowed continuous gas flow through the catalyst bed during spectra acquisition, and the sample could be heated to 673 K at a ramp rate of 60°/min. The temperature of the cell was monitored with a K-type thermocouple mounted inside the catalyst powder. All IR measurements were carried out at atmospheric pressure. The spectra were acquired at a resolution of 4 cm^{-1}, typically averaging 200 scans for steady state and 15 scans for temperature-programmed experiments within a temperature range of 4° degrees, and the temperature was ramped at 20°/min. Background spectra were obtained from samples at room temperature in a flow of H_2. All DRIFTS data were transformed into Kubelka–Munk units, which are linearly related to the adsorbed species surface concentration.

The experimental procedure followed in the combined temperature-programmed DRIFTS (TPD-IR) experiments was identical in every experimental set. Before each set of experiments the catalyst was heated under pure H_2 flow at 573 K for 30 min. Then it was cooled to room temperature, at which point H_2 flow was switched to 7% CO/He flow for 30 min. Subsequently the sample was purged with pure He flow for 2 min and then annealed under the desired gas flow (He or H_2) at a constant temperature rate of 10 K/min and a gas flow rate of 12 cm^3/min. No CO absorption bands were detected on Mo oxide, whereas TiO_2 anatase support chemisorbed CO weakly under the present experimental conditions, as confirmed by separate CO absorption experiments on these substrates. Thus it is reasonable to assume that practically only Pt provides active sites for CO adsorption.

3. Results

3.1. Characterization of Pt–Mo/TiO_2 and Pt/TiO_2 catalysts

3.1.1. Surface composition of the catalysts

Surface atomic ratios calculated from XPS peak intensities and atomic sensitivities [15], assuming uniform distribution of all elements, are compared with the nominal atomic composition to obtain information about the composition of the surface and the dispersion of the active phases. In Table 1 the nominal surface atomic ratios and the calculated (experimental) surface atomic ratios are summarized for Pt_x–Mo/TiO_2 ($x = 1, 4$) catalysts. In addition, Pt surface area, particle size, and dispersion, as derived in hydrogen chemisorption experiments, is also included only for the Pt/TiO_2 sample. The significant decrease in Pt surface area for the Pt_x–Mo samples, as discussed later, and taking into account the information from the FTIR and XPS experiments, indicates that Mo species are screening a significant portion of the Pt surface atoms. This is also corroborated by the fact that the XPS-measured Pt/Mo experimental atomic ratios are lower than the corresponding nominal atomic ratios. Nevertheless, the particle size estimated based on H_2 chemisorption measurements for the cases of Pt_x–Mo/TiO_2 samples does not correspond to the real particle size of the Pt_x–Mo particles.

3.1.2. Oxidation states of Pt and Mo

Fig. 1 depicts Pt 4f XP spectra for Pt, Pt–Mo, and Pt_4–Mo supported on TiO_2, after they have been heated at 570 K under a H_2 atmosphere. The Pt 4f spectrum of a metallurgically prepared monophase PtMo alloy [3] is also presented for comparison. The Pt 4f binding energies of Pt/TiO_2, Pt–Mo/TiO_2, and Pt_4–Mo/TiO_2 are located at 71.1, 71.6, and 70.75 eV, respectively, and the binding energy of the metallurgically prepared sample is located at 71.5 eV. The shape of the Pt 4f spectra for the TiO_2-supported samples reveals the existence of more than one Pt species. Their deconvolution, as discussed later, indicates the existence of oxidized states induced by OH^- or O species. The intensity ratio, as measured on a Pt foil, of the Pt 4f doublet components was 3:4, and their splitting energy was 3.3 eV. The locations of the major peaks of Pt $4f_{7/2}$ photoelectron spectra are 71.1, 71.48, and 70.75 eV for the cases of Pt/TiO_2, Pt–Mo/TiO_2, and Pt_4–Mo/TiO_2, respectively. Cluster size effects that can cause BE increases up to 0.7 eV are excluded because of

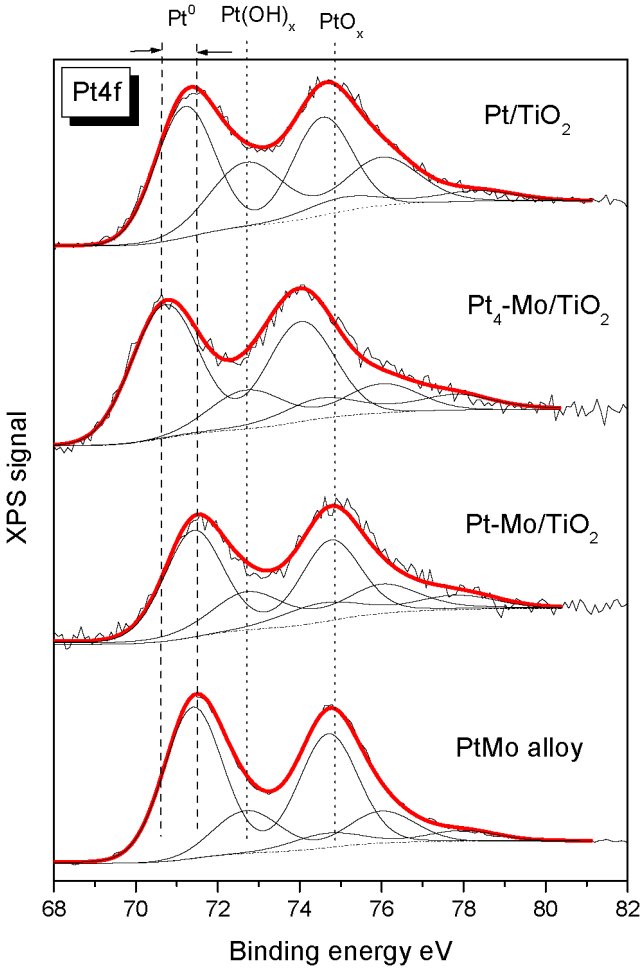

Fig. 1. Deconvoluted Pt 4f XP spectra of PtMo alloy and TiO_2 supported Pt and Pt_x–Mo catalysts.

Table 1
Pt active surface area, dispersion and mean particle size derived by hydrogen chemisorption experiments and nominal and experimentally derived atomic XPS ratios

Catalyst	Pt surface area (m^2/g)	Mean particle size (nm)	Dispersion (%)	Nominal atomic ratio		Experimental atomic ratio	
				Ti/O	Pt/Mo	Ti/O	Pt/Mo
Pt/TiO_2	1.23	8.3	14	0.5		0.42	
$Pt–Mo/TiO_2$	0.46	–	–	0.5	1	0.45	0.64
$Pt_4–Mo/TiO_2$	0.19	–	–	0.5	4	0.45	2.5

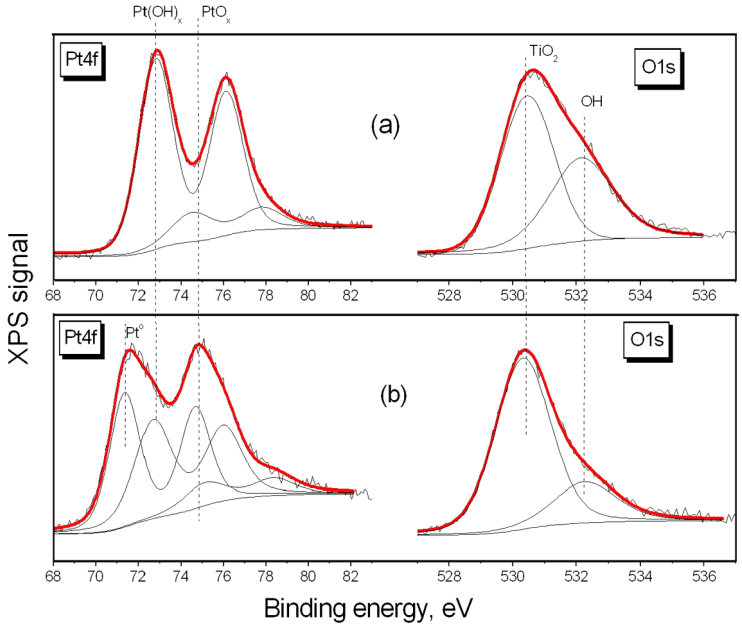

Fig. 2. Deconvoluted Pt 4f and O 1s XP spectra of 10 wt% Pt/TiO_2 catalysts before (a) and after (b) the exposure/reduction in H_2 flow at 573 K.

the rather large particle, which is larger than 2 nm [16–19]. From hydrogen chemisorption experiments the mean particle size measured for the case of Pt/TiO_2 sample is 8 nm (Table 1), and though for the case of Pt_x–Mo the estimation of the particle size is not reliable because of the screening of the Pt surface atoms from Mo species, the size of the Pt–Mo particles, as discussed further on, is not expected to be below 8 nm. Although the location of the binding energy of the major peak of Pt in the $Pt–Mo/TiO_2$ sample is very close to the corresponding peak location of the PtMo alloy, the identification of Pt in $Pt–Mo/TiO_2$ with PtMo alloy is not straightforward. Nevertheless, the variation of the binding energy of the Pt 4f major peak for the samples depicted in Fig. 1 strongly indicates the effect of Mo on the electronic properties of Pt. It is worth noticing that within the detection depth of XP measurements we did not detect any Pt species whose binding energy is located at the value of pure Pt (70.9 eV). This observation strongly indicates that Pt forms bulk solid solutions with the Mo species, which exist only as oxides (read below).

To understand the origin of the oxidation states of Pt deposited on TiO_2, XP spectra for Pt 4f photoelectrons are shown in Fig. 2a that were taken for the cases of 10 wt% Pt/TiO_2 before and after heating of the sample at 350 °C under vacuum. The binding energy of Pt 4f photoelectrons is located at 72.8 eV before H_2 reduction, and it is deconvoluted into two peaks with binding energies at 72.8 and 74.6 eV. After heating, a major Pt 4f state at 71.34 eV appears, together with the state at 72.8 eV and a smaller peak at 75.2 eV. The peak at 72.8 is attributed to Pt^{2+} because of its combination with OH^- or O species [20], and the peak at 74.6 and 75.2 is attributed to PtO_2 species [21]. Interestingly, after heating, the corresponding O 1s XP spectra show a pronounced decrease in the intensity of hydroxyl species (Fig. 2b, BE = 532.2 eV), in direct correlation with the reduction/transformation observed with Pt species (Fig. 2a). In conclusion, this experiment strongly indicates that oxidized Pt species that are formed on the TiO_2 surface are most probably originating from the diffusion (spillover) of OH^- from the TiO_2 support onto the Pt crystallites.

Fig. 3 shows Mo 3d XP spectra for the $Pt–Mo/TiO_2$ and Mo/TiO_2 catalyst (bottom curve) and the corresponding spectrum of the PtMo alloyed reference sample. As can be deduced from the shape of the Mo 3d curves for the TiO_2-supported samples, Mo exists in various Mo oxidation states overlapping at the Mo 3d region. The distribution of Mo oxidation states was estimated by deconvolution of Mo 3d spectra, displayed in the same figure. The intensity

Table 2
Intensity ratios of various Mo species derived after deconvolution of the Mo 3*d* peak

Catalyst	Mo (III)		Mo (IV)		Mo (V)		Mo(VI)	
	BE	Ratio (%)	BE	Ratio (%)	BE	Ratio (%)	BE	Ratio (%)
Mo/TiO_2			230.0	22	231.4	31	232.8	47
$Pt–Mo/TiO_2$			229.7	23	231.4	61	232.8	16
$Pt_4–Mo/TiO_2$	228.2	15	229.7	40	231.4	45		

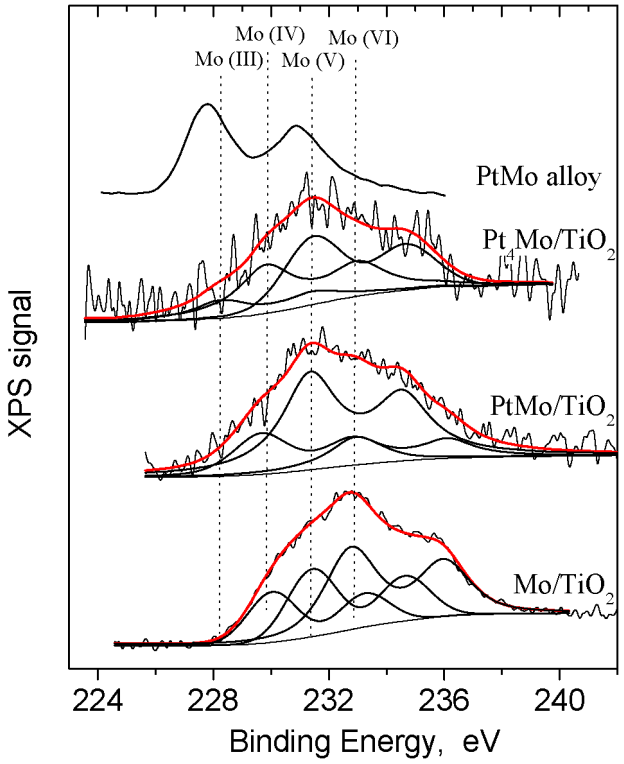

Fig. 3. Deconvoluted Mo 3*d* XP spectra of TiO_2 supported Pt_x–Mo catalysts. At the top of the graph the spectrum of a metallurgically prepared Pt_3Mo bulk alloy is also presented for comparison.

ratio of the Mo 3*d* doublet components was 2:3, and their splitting energy was 3.2 eV [15]. The results of this analysis are summarized in Table 2. Each spectrum was composed of three characteristic doublets. The Mo $3d_{5/2}$ peak at 228.2–228.4 eV may be assigned to MoO_x, where $0 < x < 4$. In particular, the Mo 3*d* peak around 228.4 eV was previously attributed to Mo^{3+} of Mo_2O_3 [22,23]. These species are detected only at a high Pt/Mo ratio, and their existence is probably due to hydrogen pretreatment [22]. The peak at 229.7 eV is characteristic of MoO_2 compounds [15,22] with the metal oxidation state Mo^{4+}. The peak at 231.3 ± 0.1 eV is the most abundant species found in all samples and may be attributed to molybdenum compounds with the metal in oxidation state Mo^{5+}, probably Mo_2O_5 or $MoO(OH)_3$ [24,25]. Finally, the component around 232.8 eV is due to Mo^{6+} states of MoO_3 [15,22]. After hydrogen pretreatment (not shown), Mo^{4+} species increase at the expense of Mo^{6+} states, in agreement with previous studies of molybdenum oxide hydrogen treatment [22]. Nevertheless, no XPS signal was observed at 227.8 eV, where the Mo 3*d* peak for PtMo alloys was found previously [3,10].

3.2. DRIFT spectroscopy study of CO absorption over Pt_x–Mo/TiO_2 and Pt/TiO_2 catalysts

3.2.1. H_2 treatment, dehydroxylation, and water desorption

Hydrogen treatment at 570 K, before CO exposure, does not show any significant reduction of TiO_2 support, as was found by XPS. However, during heat treatment, DRIFTS data for the sample under H_2 or He show gradual desorption of water and depletion of hydroxyl species mainly from the TiO_2 support. This is observed in the diminishment of the sharp peak at 1640 cm^{-1} and the broad absorption band in the range of 2500–3700 cm^{-1}, respectively, for all samples examined (spectra not shown for brevity) [30]. Exposure of the sample in He or H_2 flow again at low temperature results in the gradual development of these bands due to the restoration of water and hydroxyl groups mainly by the residual water in the flow system, although it should exist in almost undetectable concentrations.

3.2.2. CO absorption over Pt and Pt_x–Mo catalysts

DRIFTS measurements were performed to study the CO absorption on Pt–Mo supported catalysts. Fig. 4 shows the normalized IR bands of the adsorbed CO species on Pt and Pt_x–Mo catalysts supported on TiO_2. The C≡O stretching frequency on Pt has traditionally been interpreted in terms of the CO adsorption site. Frequencies in the 1950–2100 cm^{-1} region have been assigned to CO linearly coordinated to Pt sites (denoted as CO_L), and frequencies within the 1950–1750 cm^{-1} region were assigned to multibonded, bridged, and threefold bonded CO species (denoted as CO_{MB}) [26]. The adsorption of CO on cationic Pt^{n+} sites has been observed within 2184–2120 cm^{-1} [27,28]. These species, in some cases, especially when the metal particle is supported on zeolites [28], are very weakly bonded to the Pt sites, and they desorb from the surface upon evacuation at room temperature. Hadjiivanov [27] concluded that the co-adsorption of water molecules can cause the shift of the IR band of the adsorbed CO on Pt^{n+} sites from 2138 cm^{-1} to 2114 and 2088 cm^{-1}. The authors interpreted this by considering that H_2O can act as an electron donor (Lewis base) to the Pt^{n+} site, so that the electron density will increase, thus affecting the electron back-donation to the CO $2\pi^*$ antibonding orbital. Nevertheless, in the present study we did not detect any IR absorbance within the aforementioned range, though the

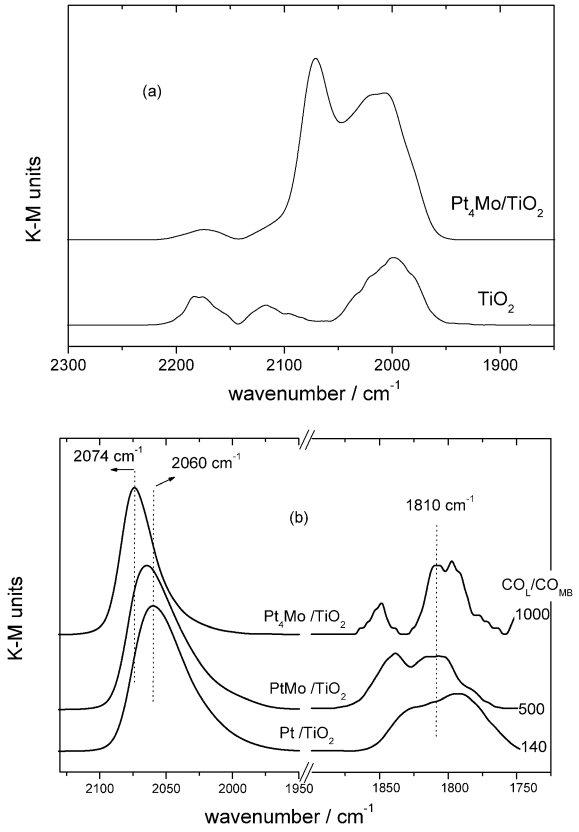

Fig. 4. (a) DRIFT spectra under 7% CO/He flow at 300 K. (b) Normalized in intensity DRIFT spectra taken at 300 K for saturation coverage of CO adsorbed on 5% Pt, Pt–Mo and Pt_4–Mo supported on TiO_2 and subsequent exposure in He for 2 min (CO_{MB} species intensity is properly normalized).

XPS experiments had shown partly reduced Pt, even after the reduction of the samples with H_2 at 350 °C. This can most probably be attributed to the coexistence of water on the catalyst surface, which may destabilize the Pt^{n+} sites or induce the shift of the band and therefore its overlapping within the range of the CO_L band that is being detected because of the CO adsorption on reduced Pt. Instead a band with a maximum around 2000 cm^{-1} (Fig. 4a) was detected under CO flow, which readily desorbs upon evacuation. These species were attributed to CO adsorption on the TiO_2 support, as the same absorption band was observed in reference experiments that were carried out on a plain TiO_2 sample.

A broad CO_L peak centered at 2060 cm^{-1} dominates the IR band of the Pt/TiO_2 catalyst in the left part of Fig. 4b after CO gas-phase evacuation. The CO_L band was blue shifted to 2064 and 2074 cm^{-1} for PtMo and Pt_4Mo, respectively. Depending on catalyst preparation and treatment, the CO_L peak band maxima for CO absorption on TiO_2-supported Pt catalysts were reported at frequencies varying between 2090 and 2050 cm^{-1} [26,29–31]. The CO_L band position is sensitive to various factors, such as catalyst dispersion, Pt particle microstructure (steps, crystal phases, etc.), and charge transfer in the vicinity of Pt adsorption sites. Thus, the increased IR peak width observed at the Pt/TiO_2 catalyst probably originates with superimposition of the various Pt sites with relatively close absorption frequencies.

The multibonded CO species is located at about 1810 cm^{-1}, as is evident from the right part of Fig. 4b. The intensity of these species was significantly lower than that of the linear species. This does not necessarily mirror the actual CO_L/CO_{MB} species proportion on the surface, since the extinction absorption coefficient of the linear species is higher than that of the bridge bonded species [32]. However, it is worth noting that the addition of Mo to the surface affects the relative CO_L/CO_{MB} proportion among the samples. In particular, with increasing Pt/Mo atomic ratio, the measured CO_L/CO_{MB} ratio increases. In other words, Mo seems to affect CO_{MB} sites to a larger extent than it does CO_L. Nevertheless, the low intensities of the IR band of the CO_{MB} species do not permit a clear view during annealing experiments and will not be interpreted below.

3.2.3. *Temperature-programmed desorption of CO under He flow*

Thermal desorption infrared experiments (TPD-IR) of CO adsorbed on Pt_x–Mo/TiO_2 and Pt/TiO_2 catalysts were carried out to get a deeper insight into the CO–Pt desorption characteristics and consequently the strength of its bond with the Pt surface. Since the DRIFTS signal depends on the penetration depth of the infrared beam into the powder sample and it is a strong function of the particle size and packing density, a direct quantitative comparison of CO coverage between the samples based on DRIFT spectra is generally not acknowledged [33]. Nevertheless, it has been found recently that there is proportionality between the IR band area of the CO_L species and its amount on the Pt surface, which does not depend on the sample temperature [34]. Quantitative studies were performed on each sample by FTIR spectroscopy at various temperatures. To compare quantitatively the trends in CO coverage between the samples during linear ramping of temperature, the ratios of the CO_L IR band intensity at a given temperature to the higher IR band intensity (I_{rel}) are illustrated graphically in Fig. 5 for all samples examined. This intensity ratio gives the relative coverage of CO_L species at each temperature.

In the case of monometallic Pt catalyst, I_{rel} goes through a maximum at 360 K and declines monotonically thereafter, approaching zero at 500 K. The derivative of the $(1 - I_{rel})$ curve represents simulated temperature-programmed desorption curves, as has been reported previously [35]. According to this procedure, the maximum CO_L desorption rate on Pt/TiO_2 is located at 420 K (see inset of Fig. 5). The main observations depicted in Fig. 5 for Pt/TiO_2 are consistent with previous findings for Pt catalysts supported on Al_2O_3 [35,36], according to which the maximum CO_L desorption rate was found in the temperature range of 390 to 420 K [35]. On the other hand, Pt–Mo/TiO_2 catalysts exhibit significantly different curve profiles, which correspond to a much faster CO_L depletion rate. In particular, the CO_L area decreases steadily without exhibiting any initial increasing

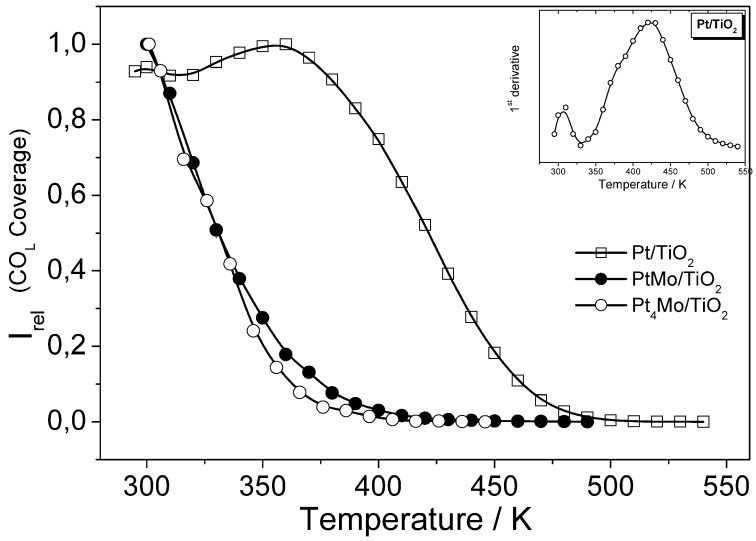

Fig. 5. CO_L peak areas normalised to the higher measured intensity as a function of annealing temperature for Pt, Pt–Mo and Pt_4–Mo supported on TiO_2 catalysts. Initially the sample was exposed to 7% CO/He for 30 min and then annealing was carried out under He flow over the catalyst. Inset: Peak area derivative of Pt/TiO_2 TPD curve.

stage or any inflection point, whereas complete desorption of CO is observed already at 370 K. In addition, the profiles obtained for the various catalysts with different Pt/Mo atomic ratios are quite similar, indicating that this factor is not decisive for the CO_L desorption profiles.

3.2.4. Temperature-programmed desorption of CO under H_2 flow

The exposure of CO_L adsorbed species in H_2 affects both its IR band position and its desorption temperature. It is worth noting that a systematic red shift of about 10 cm^{-1} for all catalysts exposed to hydrogen has been observed, and the blue shift for various Pt/Mo ratios is similar to that observed under He flow. The CO_L peak for monometallic Pt catalyst appears at 2053 cm^{-1}, whereas a pronounced blue shift, which increases up to 15 cm^{-1}, is observed for the Pt–Mo catalysts.

The evolution of the relative CO_L coverage upon sample annealing with 20 K/min under hydrogen flow is depicted in Fig. 6, where I_{rel} evolution of Pt/TiO_2 and Pt_x–Mo/TiO_2 catalysts is plotted against temperature. The CO_L species desorbs at higher temperatures from the Pt/TiO_2 sample, followed by Pt–Mo/TiO_2 and Pt_4–Mo/TiO_2, respectively. The maximum desorption rates of the CO_L species, being proportional to the derivative of $1 - I_{rel}$ with respect to temperature (similar to the inset in Fig. 5), are located at 460, 412 ± 5, and 390 ± 5 K for the Pt/TiO_2, Pt–Mo/TiO_2, and Pt_4–Mo/TiO_2 samples, respectively. It is interesting to point out that the lowest desorption temperature is observed for the sample with the lowest content of Mo (Pt_4–Mo/TiO_2) and it is 70 K below the corresponding desorption temperature of the Mo-free Pt/TiO_2 sample.

From a comparison of Figs. 5 and 6 (i.e., TPD experiments under He and H_2 flows), it is easily concluded that CO desorbs in all cases at higher temperatures under H_2 flow than it does under He flow. In the case of Pt_x–Mo catalysts the effect of hydrogen is significantly more prominent.

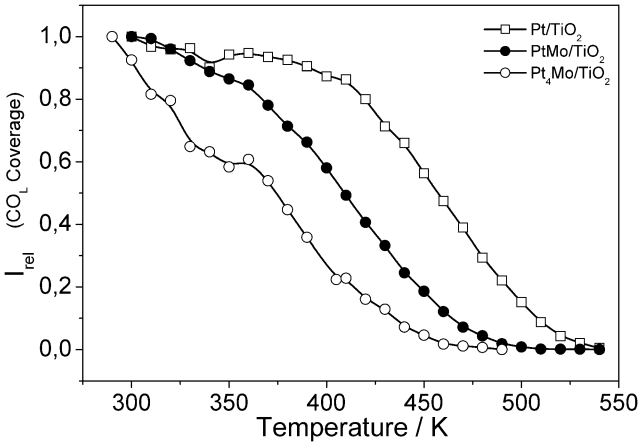

Fig. 6. CO_L peak areas normalised to the higher measured intensity as a function of the annealing temperature for Pt, Pt–Mo and Pt_4–Mo supported on TiO_2 catalysts. Initially the sample was exposed to 7% CO/He for 30 min and then annealing was carried out under H_2 flow over the catalyst.

4. Discussion

4.1. Arrangement and electronic interaction between Pt and Mo on TiO_2 support

To be in the position to discuss and conclude on the origin of the catalytic and specifically the adsorption/desorption properties of Pt_x–Mo/TiO_2 catalysts, the arrangement and interaction of the various components on the support should be clarified. The main experimental observations based on XPS, DRIFTS, and chemisorption experiments can be summarized as follows:

Table 3
Nominal and experimental atomic ratios of Pt between Pt/TiO_2 and Pt_x–Mo/TiO_2 samples with total metal loading 5 wt%

Catalyst	$[Pt/Ti]_{Pt/TiO_2}/[Pt/Ti]_{Pt_x-Mo/TiO_2}$		$[Pt/Mo]_{nom}/[Pt/Mo]_{exp}$
	Nominal	Experimental	
Pt/TiO_2	1	1	
Pt–Mo/TiO_2	1.49	1.47	1.56
Pt_4–Mo/TiO_2	1.12	1.14	1.6

nom, nominal; exp, experimental based on XPS measurements.

1. Pt $4f$/Ti $2p$ XPS signal ratios vary proportionally with increasing Mo content, thus indicating that the dispersion of Pt on the TiO_2 support remains constant (Table 3).
2. Significant difference is observed between the IR CO_L band intensities of the Pt/TiO_2 and Pt_x–Mo/TiO_2 samples, which, in combination with the corresponding Pt surface area shown in Table 1, indicates that Mo is screening a significant part of the Pt surface atoms.
3. The systematically lower experimental Pt/Mo atomic ratios as compared with the nominal ones indicate that Mo segregates on the Pt crystallite surface.
4. Although according to the aforementioned consideration Mo oxide species may cover a significant portion of the Pt surface, the Pt $4f$ signal is not attenuated with increasing Mo content (constant $(Pt/Mo)_{nom}/(Pt/Mo)_{exp}$, where nom = nominal, exp = experimental, Table 3). Based on this observation, we are driven to the conclusion that Mo is finely dispersed on the Pt crystallite surface, probably in two-dimensional nanoclusters.
5. As shown in Table 2, the Mo species exist in several oxidation states, ranging between Mo(III)–Mo(V) on Pt_4–Mo/TiO_2 and Mo(IV)–Mo(VI) in Pt–Mo/TiO_2, thus indicating the effect of Pt on the distribution of the Mo oxidation states.
6. The bulk variation of the binding energy of the Pt $4f$ core level peaks (Fig. 1) for the two Pt_x–Mo samples shows that bulk interaction takes place between Mo oxide species and Pt, indicating the formation of solid solution between the two species.

Summarising the aforementioned considerations, it is reasonable to assume that Pt forms a solid solution with Mo oxide species. These particles are dispersed on the TiO_2 surface, while upon them oxidized Mo aggregates are deposited in a two-dimensional cluster arrangement. Thus an extended effect on the electronic properties of Pt is expected to affect its chemisorptive and in general catalytic properties.

4.2. Thermal desorption of CO under He and H_2 atmospheres

Several researchers in the past proposed that the promoting role of Mo on Pt for its high CO tolerance is due to its oxogenic nature, which, especially in the form of $MoO(OH)_3$, can easily supply OH species that can readily oxidize CO adsorbed species on Pt [10,25,37]. Based on this conclusion and taking into account the evidence from the XPS measurements (Fig. 3) that the main oxidation state of Mo is most probably related to $MoO(OH)_3$, it is quite reasonable to assume that the complete depletion of CO_L species even below 370 K for the case of Pt_x–Mo samples (Fig. 5) can be due to its oxidation by the highly active OH species supplied by $MoO(OH)_3$ at the boundaries of the MoO_x clusters that are distributed on the Pt surface. The high dispersion of Mo species on the Pt particles results in a highly extended Mo oxide-Pt-gas phase three phase boundaries and consequently in a significant increase in the reaction zone [38].

As depicted in Figs. 5 and 6, the desorption behavior of CO_L under He flow (Fig. 5) is quite different from that observed under H_2 flow (Fig. 6). In all cases, under H_2 flow, the CO_L desorption temperature increases even by 100 K, especially in the case of Pt_x–Mo samples. To understand this behavior it is reasonable to expect the interaction of the exposed samples in H_2 atmosphere to result either in the reduction of the catalysts surface or in the hydrogenation of the CO_L species. The latter consideration can be excluded, since adsorbed CO species under H_2 flow desorb in all cases at temperatures higher than the corresponding desorption temperatures under He flow. In this respect, as will be discussed further on, the effect of H_2 is more likely to correlate with the reduction of the Pt surface. Considering that H_2 is competitively reacting with the same oxidic species that react with and oxidize CO_L, it can be easily understood why CO_L species desorbs at significantly higher temperatures, as depicted in Fig. 6.

It is worth noticing that in the case of Pt_4–Mo, in the CO_L desorption curve of Fig. 6, two regions can be observed. The low-temperature desorption region, which is extended to 350 K, has characteristics similar to those of the corresponding curves of Fig. 5 obtained under He flow. This can be attributed to the oxidation of CO_L species situated at the boundaries of the Mo oxide species. In contrast, in the high-temperature region, the CO_L species, which are most probably situated at a critical distance from the Mo oxide boundaries, desorbs from the Pt surface at a higher temperature. This can be realized in terms of the longer characteristic diffusion time needed to approach the Mo oxide boundaries in comparison with the corresponding characteristic reaction time of H_2 with the hydroxyl species originating from the $MoO(OH)_3$. The aforementioned consideration, in accordance with the above discussion on the structural arrangement of the Pt and Mo phases, is also supported by the fact that among the three samples, Pt_4–Mo shows the highest coverage by the Mo oxide species and most probably the highest ratio between the boundary length and the free Pt surface.

In the case of the Pt/TiO_2 sample, the ~ 33 K increase in the CO_L desorption temperature cannot be attributed to oxidation and desorption processes, under He and H_2 respectively, as in the aforementioned cases of Pt_x–Mo samples. Under He and H_2 flows the main depletion process of the

CO_L species is their desorption from the surface. Thus, as discussed further on, the difference in the desorption temperatures under He and H_2 flows shows strengthening of the Pt–CO adsorption bond, which is induced under H_2 flow due to metal support interactions.

The effect of Mo oxide species on the modification of the chemisorptive properties of Pt can be deduced by the fact that CO desorption from the Pt_4–Mo/TiO_2 sample under H_2 flow takes place approximately 70 K below the corresponding desorption temperature for the Pt/TiO_2 sample (Fig. 6). Thus in the case of the Pt_4–Mo/TiO_2 sample, CO_L species are less strongly bonded on the Pt surface atoms.

The aforementioned observations are corroborated by the corresponding IR band shifts of the linearly adsorbed CO. As depicted in Fig. 4b, the blue shift by 14 cm^{-1} observed for the case of Pt_4–Mo/TiO_2 denotes a less strongly bonded CO molecule on the Pt surface, and the corresponding red shift under H_2 flow denotes a more strongly bonded CO. The CO bonding strength with the Pt surface is mainly determined by the dipole moment that develops because of the back-donation of electrons from the metal to the $2\pi^*$ antibonding orbital of the carbon/oxygen bond. Thus the higher the degree of electron back-donation, the stronger is the bond strength of linearly adsorbed CO_L on the Pt surface, and the corresponding IR band is shifted toward lower wavenumbers because of the weakening of the carbon/oxygen bond [27,39]. These observations are in good agreement with other electrochemical studies in the literature, which show that Pt_4Mo composition exhibits the highest tolerance in CO poisoning among all Pt–Mo compositions [11].

4.3. Metal support interaction (SMSI)

In a recent publication Wahlström et al. [40] reported on the nature of bonding of Au nanoclusters on rutile TiO_2, thus providing a deeper insight into the ability of TiO_2 to develop strong and effective metal support interactions. From a combination of scanning tunneling microscopy (STM) and density functional theory (DFT) calculations, they concluded that Au nanoclusters are more effectively bonded on the TiO_2 support when they are combined with existing O vacancies on the TiO_2 substrate. In this respect the exposure of the catalyst under redox conditions, which can affect the concentration of the O vacancies, is expected to induce chemical and structural alterations in the properties of the supported metal nanoparticles. Certainly these oxygen vacancies are accompanied by the partial surface reduction of Ti^{4+}, which in the present study could not be detected by XPS, most probably because of the low sensitivity of the technique, which is caused by the overlap of the strong signal of Ti $2p$ from the bulk of the TiO_2 support.

Another very interesting approach concerning SMSI has been reported in a comprehensive study by Vayenas and coworkers [41,42], who have explicitly reported that the nature and origin of the SMSI effect on ionic supports like TiO_2, ZrO_2, or CeO_2 is due to the back-spillover of O^{2-} ions onto the metal crystallites, so that the Fermi level of the supported metal catalyst is aligned with that of the support. These ionic oxidic species form an active double layer, with the metal surface acting as a promoter for the supported metal catalysts, thus inducing an increase in their work function, especially at temperatures where the mobility of O^{2-} ions is high enough.

Beyond the migration and spillover of O^{2-} ions, a similar mechanism and driving force can also be understood and be applicable, at lower temperatures, in the case of hydroxyl ionic (OH^-) species, which are adsorbed on various oxide surfaces and are characterized by different surface mobilities and adsorption strengths, depending on the nature of the oxide. TiO_2 or even more molybdenum oxides are characterized by the fact that they can accommodate large quantities of hydroxyl ionic species, which exhibit high mobility and consequently a high spillover effect on Pt metal crystallites [43], compared with SiO_2 and Al_2O_3. As indicated by IR and XPS spectroscopy, the depletion of hydroxyl species OH^- from the catalyst surface is accompanied by the partial reduction of the deposited Pt particles (Fig. 2) at temperatures below 520 K, whereas in the case of SiO_2 and Al_2O_3 their desorption takes place above 870 K.

In a way similar to the case of O^{2-}, the spillover of OH^- species on the Pt surface and the formation of an active double layer of OH^- with Pt surface atoms is expected to induce such alterations in the work function or correspondingly in the Fermi edge of Pt so that the electron back-donation on the CO_{ad} molecule is significantly affected (through the metal interactions). Thus it is expected that the aforementioned active double layer, as in the case of the O^{2-} double layer of catalysts deposited on ionic supports [42,43], will cause a decrease in the Fermi level or, correspondingly, an increase in the work function of the Pt surface. Consequently it is assumed that the bonding strength of the CO_{ad} molecule, as an electron acceptor, will become weaker, resulting in a decrease in the degree of electron back-donation onto the antibonding orbital of the CO_L, thus inducing an IR band shift toward higher wavenumbers. This is true if we consider the 10 cm^{-1} red shift of the CO_L IR band when changing the flow from He to H_2. Furthermore, the 14 cm^{-1} blue shift in the IR band that is observed for the Pt_4–Mo/TiO_2 sample can also be attributed to the oxogenic nature of Mo and its ability to promote OH^- spillover onto the Pt surface and to the interaction of Mo oxides with the Pt surface.

Certainly the survival of OH_{ad} on the Pt surface is quite limited, since it is directly reacting to the production of H_2O and O_{ad}. However, the reactivity of the OH^- species is expected to be significantly lower than that of the normally adsorbed OH_{ad}, so that an effective double layer can be formed that may induce changes in the electronic properties of Pt. The promoting role of OH^- was shown in electrochemical promotion experiments, where the positive polarization of a Pt black gas diffusion electrode immersed in KOH aqueous electrolyte induced significant promotion of the catalytic activity of the Pt electrode/catalyst [44,45].

5. Conclusions

Although we cannot say for sure which of the aforementioned models is the most suitable for explaining the IR results, the truth certainly lies within a synthesis and combination of the aforementioned models and ideas. Therefore, according to the above-described experimental results, we can deduce that Mo oxides and Pt are probably in intimate contact with each other either through the formation of solid solutions or through the distribution of Mo oxide on the Pt particles surface. In this respect, Mo oxide species may promote the oxygen or hydroxyl spillover onto the Pt surface, which can readily react at the Mo oxide–Pt boundaries with CO toward CO_2 formation or can induce modifications on the electronic properties of Pt, thus affecting the strength of the chemisorptive bond of CO_L species with the Pt surface atoms.

Acknowledgment

This work was supported by the EESD program of the European Commission under contract ENK5-CT-2001-00572.

References

[1] U. Diebold, Surf. Sci. Rep. 48 (2003) 53.
[2] C. Song, Catal. Today 77 (2002) 17.
[3] S.G. Neophytides, S.H. Zafeiratos, M.M. Jacksic, J. Electrochem. Soc. 150 (2003) E512.
[4] J. Shim, C.-R. Lee, H.-K. Lee, J.-S. Lee, E.J. Cairns, J. Power Sources 102 (2001) 172.
[5] N.M. Markovic, P.N. Ross Jr., Surf. Sci. Rep. 45 (2002) 117.
[6] M. Watanabe, S. Motoo, J. Electroanal. Chem. 60 (1975) 275.
[7] J.C. Davies, B.E. Hayden, D.J. Pegg, Surf. Sci. 467 (2000) 118.
[8] M.M.P. Janssen, J. Moolhuysen, J. Catal. 46 (1977) 289.
[9] T. Frelink, W. Visscher, J.A.R. Vanveen, Surf. Sci. 335 (1995) 353.
[10] B.N. Grgur, N.M. Markovic, P.N. Ross Jr., J. Phys. Chem. B 102 (1998) 2494.
[11] B.N. Grgur, N.M. Markovic, P.N. Ross Jr., J. Electrochem. Soc. 146 (1999) 1613.
[12] T.E. Shubina, M.T.M. Koper, Electrochimica Acta 47 (2002) 3621.
[13] Y. Ishikawa, M.S. Liao, C.R. Cabrera, Surf. Sci. 513 (2002) 98.
[14] V. Papaefthimiou, A. Siokou, S. Kennou, J. Appl. Phys. 91 (2002) 4213.
[15] D. Briggs, M.P. Seah (Eds.), Practical Surface Analysis, vol. 1, second ed., Wiley, New York, 1990, p. 201.
[16] R.M. Walton, D.J. Dwyer, J.W. Schwank, J.L. Gland, Appl. Surf. Sci. 125 (1998) 187.
[17] K.D. Schierbaum, S. Fischer, M.C. Torquemada, J.L. Segovia, E. Roman, J.A. Martin-Gago, Surf. Sci. 345 (1996) 261.
[18] H.-J. Steinruck, F. Pesty, L. Zhang, T.E. Madey, Phys. Rev. B 51 (1995) 2427.
[19] S. Fischer, K.-D. Schierbaum, W. Gopel, Sensors and Actuators B 31 (1996) 13.
[20] M. Peuckert, F.P. Coenen, H.P. Bonzel, Electrochim. Acta 29 (1984) 1305;
J.E. Drawdy, G.B. Hoflund, S.D. Gardner, E. Yngvadottir, D.R. Schryer, Surf. Interface Anal. 16 (1990) 369.
[21] J.P. Contour, G. Mouvier, M. Hoogewijs, C. Leclere, J. Catal. 48 (1977) 217.
[22] J.-G. Choi, L.T. Thompson, Appl. Surf. Sci. 93 (1996) 143.
[23] Y.C. Lu, C.R. Clayton, Corros. Sci. 29 (1989) 927.
[24] C.O.A. Olsson, H.J. Mathieu, D. Landolt, Surf. Interface Anal. 34 (2002) 130.
[25] S. Mukerjee, R.C. Urian, Electrchim. Acta 47 (2002) 3219.
[26] K. Tanaka, J.M. White, J. Catal. 79 (1983) 81.
[27] K.I. Hadjiivanov, J. Chem. Soc., Faraday Trans. 94 (13) (1998) 1901.
[28] A.Yu. Stakheev, E.S. Shpiro, O.P. Tkachenko, N.I. Jaegery, G. Schulz-Ekloffy, J. Catal. 169 (1997) 382.
[29] J. Rasko, J. Catal. 217 (2003) 478.
[30] V.E. Benvenutti, L. Franken, C.C. Morro, C.U. Davanzo, Langmuir 15 (1999) 8140.
[31] H. Einaga, M. Harada, S. Futamura, T. Ibusuki, J. Phys. Chem. B 107 (2003) 9290.
[32] M.A. Vannice, C.C. Twu, J. Chem. Phys. 75 (1981) 5944.
[33] M.M. Schubert, M.J. Kahlich, H.A. Gasteiger, R.J. Behm, J. Power Sources 84 (1999) 175.
[34] A. Bourane, O. Dulaurent, D. Bianchi, J. Catal. 195 (2000) 406.
[35] R. Barth, R. Pitchai, R.L. Anderson, X.E. Verykios, J. Catal. 116 (1989) 61.
[36] A. Bourane, O. Dulaurent, K. Chandes, D. Bianchi, Appl. Catal. A: Gen. 214 (2001) 193.
[37] B.N. Grgur, G. Zhuang, N.M. Markovic, P.N. Ross Jr., J. Phys. Chem. B 101 (1997) 3910.
[38] G.A. Somorjai, in: Introduction to Surface Chemistry and Catalysis, Wiley, 1994, p. 490.
[39] B. Hammer, Y. Morikowa, J.K. Norskov, Phys. Rev. Let. 76 (1996) 2141.
[40] E. Wahlström, N. Lopez, R. Schaub, P. Thostrup, A. Rønnau, C. Africh, E. Lægsgaard, J.K. Nørskov, F. Besenbacher, Phys. Rev. Let. 90 (2) (2003), 026101-1.
[41] C.G. Vayenas, S. Brosda, C. Pliangos, J. Catal. 216 (2003) 487.
[42] C.G. Vayenas, S. Bebelis, C. Pliangos, S. Brosda, D. Tsiplakides, in: Electrochemincal Activation of Catalysis, Kluwer Academic/Plenum, New York, 2001.
[43] P.L.J. Gunter, J.W. Niemantsverdriet, F.H. Ribeiro, G.A. Somorjai, Catal. Rev.-Sci. Eng. 39 (1997) 77.
[44] S.G. Neophytides, D. Tsiplakides, P. Stonehart, M.M. Jaksic, C.G. Vayenas, J. Phys. Chem. 100 (1996) 14803.
[45] S.G. Neophytides, D. Tsiplakides, P. Stonehart, M.M. Jaksic, C.G. Vayenas, Nature 370 (1994) 45.